



Sharif University of Technology  
**Scientia Iranica**  
*Transactions B: Mechanical Engineering*  
<http://scientiairanica.sharif.edu>



Research Note

# Performance of a linear controller in the nonlinear model of drug and virus delivery in cancer chemovirotherapy: A comparison between continuous and discrete approaches

M. Mobaraki\* and H. Moradi

*School of Mechanical Engineering, Sharif University of Technology, Tehran, Iran.*

Received 6 March 2021; received in revised form 31 August 2022; accepted 31 October 2022

## KEYWORDS

Cancer treatment;  
 Chemovirotherapy;  
 Tracking control;  
 Continuous & discrete models;  
 Optimal treatment;  
 Stability analysis.

**Abstract.** Best cancer treatment should reduce the density of tumor in a minimum time with few side effects, considering the input limitations. In this paper, a tracking controller was designed to achieve the mentioned objectives, simultaneously. An Ordinary Differential Equations (ODEs) based mathematical model of a human body under chemovirotherapy was selected, which included the uninfected and infected tumor cells, free viruses, immune cells, and a chemotherapeutic drug. Stability analysis was employed to determine the sensible equilibrium points. For tracking purposes, a servo controller based on the Entire Eigenstructure Assignment (EESA) approach was applied to the model, continuously and discretely. By regulating the command input properties, an optimal treatment duration with limited drug dosage and virus dosage was determined. The results indicated that the discrete controller performed smoother than the continuous controller. Thus, an optimal discrete treatment schedule with optimum duration of drug and virus delivery was proposed.

© 2023 Sharif University of Technology. All rights reserved.

## 1. Introduction

Cancer is one of the most prominent life-threatening diseases. More than three-quarters of the 20.4 million premature deaths are related to Noncommunicable Diseases (NCDs), and cancer is the cause of 30% of NCDs deaths [1]. Cancer patients struggle with physical, emotional, and financial impacts of the illness

[2]. Then, selecting the best treatment can improve human health and reduce the financial concerns [3].

Chemotherapy is one of the adjuvant treatments that can eradicate the tumors after the surgery. Long-term and high-dose drug intake can result in drug resistance and toxicity, respectively. Therefore, optimal drug schedule is vital to chemotherapy. In [4], an experiment on 905 colon cancer patients was conducted to examine the effectiveness of drug frequency (semimonthly and monthly) and treatment duration (24 and 36 weeks). They reported that the drug's high frequency reduced the toxicity, with no impact on treatment duration. They also revealed that long-term treatment would reduce drug dosage.

Virotherapy is another cancer treatment with

\*. Corresponding author. Tel.: +98 21 66165545;  
 Fax: +98 21 66000021  
 E-mail addresses: [mobaraki.mobina@mech.sharif.edu](mailto:mobaraki.mobina@mech.sharif.edu) (M. Mobaraki); [hamedmoradi@sharif.edu](mailto:hamedmoradi@sharif.edu) (H. Moradi)

great tolerance in patients. It employs oncolytic viruses to infect and lyse tumor cells. The viruses stimulate the immune cells against tumor cells and colonize multiple distant tumor sites.

The emergence of chemovirotherapy, which is the combination of chemotherapy and virotherapy, can enhance the survival probability by reducing the drug dosage and increasing the tumor infection rate [5]. Research on chemovirotherapy reported that the kind of oncolytic viruses, cancer type targeted, drug combination used, treatment duration, drug frequency, and dosage would play the most important role in combination therapy [6]. Although most studies on chemovirotherapy are conducted in a preclinical area [7,8], recent experimental and theoretical research exhibits interesting results [9–11].

Developing mathematical models to predict the tumor behavior can be time and cost efficient in comparison with experimental tests. The existing models can be classified from the viewpoint of cancer hallmarks [12]. Moreover, a review of existing non-spatial mathematical models was conducted in [13]. Several models were developed to explain the dynamics of chemotherapy [14–18] and virotherapy [19–22]. Malinzi et al. [23] in 2017 suggested the parabolic nonlinear Partial Differential Equations (PDEs) that demonstrate the dynamics of tumor cells under chemovirotherapy. Their model simulated the uninfected and infected tumor cells, a free virus, and chemotherapeutic drug. They reported chemovirotherapy to be more effective than chemotherapy or virotherapy alone. They improved their model by adding immune cells and evaluating the effect of drug fusion [11].

To determine the optimal treatment schedule, the optimal control approach was defined [24]. There are 3 different optimal approaches to solving the prepared models: analytical, approximation, and heuristic solutions [25]. Other methods like the ones in [26] used the stochastic model to maximize the probability of successfully treating cancer with no toxicity.

Although various combination cancer therapies have been investigated, designing the optimal schedule is an open question due to high nonlinearity and complexity in the models. Therefore, developing an easy-to-solve mathematical model with sensible results is necessary. Moreover, designing optimal approaches to solve these models and satisfy the treatment objectives can have a great impact on experimental cancer treatments.

In this paper, a tracking controller based on Entire Eigenstructure Assignment (EESA) method is designed to reduce the density of the tumor with a minimum time duration, limited drug, and virus dosage. A recently developed mathematical model of avascular tumor cells by Malinzi et al. [27] is considered that simulates the effect of immune cells. Then, the discrete

and continuous controllers are applied to the nonlinear model. Finally, treatment duration, command tracking properties, and sampling instant for discretizing are discussed as effective factors, which contribute to the smoothness of the closed-loop system response.

## 2. Mathematical model of cancer chemovirotherapy

One of the most efficient ways to simulate and predict the tumor's behavior is to extract an optimal mathematical model. The model nonlinearities result in a complex solution. Deriving the optimal model that comprises complexities and realities is still an open question.

### 2.1. Model descriptions and assumptions

In this paper, Malinzi's model [27] is selected and it consists of 6 states of avascular tumor cells. The model simulates the infected and uninfected tumor cells, free viruses, drug concentration, and immune cells under chemovirotherapy treatment.

The model is divided into three parts: virotherapy, immune cells, and chemotherapy. First, a fundamental model was proposed in [28] to represent the infected and uninfected tumor cells in the presence of virotherapy as:

$$\frac{dx}{dt} = xF(x, y) - \beta yG(x, y), \quad (1)$$

$$\frac{dy}{dt} = \beta yG(x, y) - ay, \quad (2)$$

where  $x$  and  $y$  represent the uninfected and infected tumor cells, and  $F$  and  $G$  are the functions that describe the growth properties of  $x$  and  $y$ , respectively.  $\beta$  and  $ay$  are infectivities of the virus and the rate of infected tumor cell death.

Free virus actions and virus burst size are essential for the dynamics of virotherapy. A virus burst size is a number of newly released viruses during the lysis of an infected cell. Malinzi's model is based on Ordinary Differential Equations (ODEs) [29], considering both virus burst size ( $b$ ) and free viruses ( $v$ ).

$$\frac{dx}{dt} = \lambda x \left( 1 - \frac{x + y}{K} \right) - \beta xv, \quad (3)$$

$$\frac{dy}{dt} = \beta xv - \delta y, \quad (4)$$

$$\frac{dv}{dt} = b\delta y - \beta xv - \gamma v. \quad (5)$$

The tumor growth in Eqs. (3)–(5) is modeled by the logistic growth and  $K$  is the maximum tumor size.  $x, y, \delta, \gamma, \lambda$ , and  $\beta$  are the population of uninfected and infected tumor cells, the rating of infected tumor

cells, free virus death, the tumor growth rate, and the inactivity of the virus, respectively.

Second, the effect of immune cells is simulated. A model was presented [30] that demonstrated the interaction between the tumor ( $T$ ) and immune cells ( $E$ ) as follows:

$$\frac{dE}{dt} = s + \frac{pET}{g+T} - mET - dE, \tag{6}$$

$$\frac{dT}{dt} = aT(1 - bT) - nET. \tag{7}$$

In our selected model, Eqs. (3) and (4) consider  $T$  as the summation of uninfected and infected tumor cells. Eq. (6) indicates the relationship between the immune cells and tumor cells, where  $s$  is the constant input,  $\frac{pET}{g+T}$  represents the effect of tumor cells on immune cells, and  $m$  and  $d$  are also the rates at which the immune cells are killed by the tumor cells and natural death of immune cells, respectively. In addition,  $a, b,$  and  $n$  are tumor growth rate, tumor decay rate, and lysis rate of tumor by immune cells, respectively.

Third, the effect of drug concentration is considered. Drug infusion per day is assumed to be constant. In our selected model, drug concentration reduces the infected and uninfected tumor cells by the Michaelis-Menten form. The change of free viruses, which reduce the uninfected tumor cells and increase the free ones, is based on Michaelis-Menten.

**2.2. Model equations**

The selected model [27] is represented through Eqs. (8) to (13):

$$\begin{aligned} \frac{dU}{dt} = \alpha U \left( 1 - \frac{U+I}{K} \right) - \frac{\beta UV}{K_u + U} \\ - \nu_U U E_T - \frac{\delta_U UC}{K_c + C}, \end{aligned} \tag{8}$$

$$\frac{dI}{dt} = \frac{\beta UV}{K_u + U} - \delta I - \nu_I E_T I - \tau E_\nu I - \frac{\delta_I IC}{K_c + C}, \tag{9}$$

$$\frac{dV}{dt} = b\delta I - \frac{\beta UV}{K_U + U} - \gamma V, \tag{10}$$

$$\frac{dE_\nu}{dt} = \phi I - \delta_\nu E_\nu, \tag{11}$$

$$\frac{dE_T}{dt} = \frac{\beta_T(U+I)}{k+(U+I)} - \delta_T E_T, \tag{12}$$

$$\frac{dC}{dt} = g(t) - \psi C, \tag{13}$$

$U, I, V, E_\nu, E_T,$  and  $C$  are the states representing the uninfected and infected tumor cells density, free viruses, virus immune cells, tumor immune cells, and drug concentration, respectively. The unit of  $U, I, V, E_\nu,$  and  $E_T$  includes cells per  $\text{mm}^3$  and  $C$  is in Nanograms per  $\text{mm}^3$ .

Eq. (8) describes the rate of changes in the density of the uninfected tumor cell. The first two parts are from Eq. (3) and represent the logistic tumor growth and effect of free viruses on the density reduction of uninfected tumor. This reduction is based on Michaelis-Menten approach that is represented by  $K_u$ . The third part demonstrates the role of tumor immune cells in reducing  $U$ . The last part shows how chemotherapeutic drug can be reduced based on Michaelis-Menten method. The parameters in Eq. (8) are described in Table 1.

Infecting tumor cells by viruses can increase the density of infected tumor cells, which is simulated by the first part of Eq. (9). The following parts discuss the reduction of infected tumor cells affected by natural death, tumor immune cells, virus immune cells, and chemotherapeutic drug. The new parameters in Eq. (9) are shown in Table 2.

Eq. (10) is inspired from Eq. (5) and represents the free virus change rate. The parameter  $b$  represents the virus burst size; thus, the first part belongs to the virus proliferation. The remaining parts demonstrate the free virus decay by the uninfected tumor cells and virus lifespan. New parameters in this equation are described in Table 3.

**Table 1.** Parameters of Eq. (8) and their description and values.

Symbol	Description	Value & units	Ref.
$K$	Tumor carrying capacity	$10^6$ cells per $\text{mm}^3$	[41]
$\alpha$	Tumor growth rate	0.206 per day	[41]
$\beta$	Infected rate of tumor cells	0.001–0.1 per day	[41]
$\delta_U$	Lysis rate of $U$ by the drug	50 per day	[31]
$K_U$	Michaelis-Menten constants	$10^5$ cells per $\text{mm}^3$	[42]
$K_c$	Michaelis-Menten constants	$10^5$ Nanograms per $\text{mm}^3$	[42]
$\nu_U$	Lysis rate of $U$ by $E_T$	0.08 $\text{mm}^3$ per cell per day	Current research

**Table 2.** Parameters of Eq. (9) and their description and values.

Symbol	Description	Value & units	Ref.
$\delta$	Infected tumor cells death	0.5115 per day	[41]
$\delta_I$	lysis rate of $I$ by the drug	60 per day	[31]
$\nu_I$	lysis rate of $I$ by $E_T$	0.1 mm <sup>3</sup> per cell per day	Current research
$\tau$	lysis rate of $I$ by $E_\nu$	0.2 mm <sup>3</sup> per cell per day	Current research

**Table 3.** Parameters of Eq. (10) and their description and values.

Symbol	Description	Value & units	Ref.
$\gamma$	Rate of virus decay	0.01 per day	[41]
$b$	Virus burst size	0–1000 virions	[43]

**Table 4.** Parameters of Eqs. (11) and (12) and their description and values.

Symbol	Description	Value & units	Ref.
$\phi$	$E_\nu$ production rate	0.7 per day	[44]
$\beta_T$	$E_T$ production rate	0.5 cells per mm <sup>3</sup> per day	[45,46]
$\delta_\nu, \delta_T$	Immune decay rates	0.01 per day	[45,46]
$k$	Michaelis-Menten constants	10 <sup>5</sup> cells per mm <sup>3</sup>	[42]

Eqs. (11) and (12) are derived from Eq. (6). The effects of constant input ( $s$ ) and tumor cells on immune cells ( $m$ ) are assumed to be insignificant. Table 4 shows the new parameters in Eqs. (11) and (12).

Eq. (13) corresponds to the drug concentration. The first part ( $g(t)$ ) and the second part represent the drug infusion into the body and drug decay.  $\psi$  represents the rate of drug decay, which is 4.17 [31].

**2.3. Equilibrium points of the model**

Different equilibrium points are calculated by changing the initial conditions. Two equilibrium points as the experimentally meaningful ones and their eigenvalues are shown in Tables 5 and 6, respectively. In the first one, changes to the states are at zero and Eqs. (8) to (13) are solved by the fourth-order Runge-Kutta method using MATLAB. In the second one, the open-loop system is simulated and the values of the steady states are determined. States in the open-loop system converge to a stable equilibrium point in a steady-state condition.  $x_1, x_2, x_3, x_4, x_5,$  and  $x_6$  are  $U, I, V, E_\nu, E_T,$  and  $C$  in Eqs. (14)–(19), respectively.

Upon comparing the stability levels of the two equilibrium points, the real eigen values of the second equilibrium point are negative, while  $\lambda_4$  of the first equilibrium point has a positive real value. Thus, based on the Liapunov indirect method, the nonlinear system is locally stable around the second equilibrium point.

In the next section, a linear controller in the nonlinear system around the selected equilibrium point is applied. Therefore, the designed controller is valid when the treatment starts near the equilibrium point.

**3. Design of the tracking controller for continuous & discrete models**

A tracking controller is applied based on EESA approach in the nonlinear model, continuously and discretely. An optimal drug and virus delivery schedule is presented with a minimum treatment duration. Our plant inputs are  $u_1(t)$  and  $u_2(t)$ , which are the supply of viruses and drug dosage from external sources. Dynamic equations of the plant are explained by Eqs. (14) to (19) as follows:

$$\frac{dU}{dt} = \alpha U \left( 1 - \frac{U + I}{K} \right) - \frac{\beta UV}{K_U + U} - \nu_U U E_T - \frac{\delta_I IC}{K_c + C}, \tag{14}$$

$$\frac{dI}{dt} = \frac{\beta UV}{K_U + U} - \delta I - \nu E_T I - \tau E_\nu I - \frac{\delta_I IC}{K_c + C}, \tag{15}$$

$$\frac{dV}{dt} = b\delta I - \frac{\beta UV}{K_U + U} - \gamma V + u_1(t), \tag{16}$$

**Table 5.** Two equilibrium points of the selected nonlinear model of the Chemovirotherapy.

1st equilibrium point (obtained from equations)						2nd equilibrium point (open-loop endpoints)					
×1	×2	×3	×4	×5	×6	×1	×2	×3	×4	×5	×6
5233.45	0	0	0	2.49	11.99	4357	3.13	6.61e4	219	2.09	11.99
$A = \begin{bmatrix} -0.00107 & -0.001 & -0.002511 & 0 & -418.6764 & -2.6161 \\ 0 & -0.7673 & 0.002511 & 0 & 0 & 0 \\ 0 & 255.75 & -0.01251 & 0 & 0 & 0 \\ 0 & 0.7 & 0 & -0.01 & 0 & 0 \\ 0.0000045 & 0.0000045 & 0 & 0 & 0 & -4.17 \\ 0 & 0 & 0 & 0 & 0 & 0 \end{bmatrix}$						$A = \begin{bmatrix} 0.00043 & -0.0008975 & -0.0021 & 0 & -348.57 & -2.178 \\ 0.0306 & -44.53 & 0.0021 & 0 & -0.3129 & -0.00187 \\ -0.0306 & 225.75 & -0.0121 & 0 & 0 & 0 \\ 0 & 0.7 & 0 & -0.01 & 0 & 0 \\ 0.0000045 & 0.0000045 & 0 & 0 & -0.01 & 0 \\ 0 & 0 & 0 & 0 & 0 & -4.17 \end{bmatrix}$					
$B = \begin{bmatrix} 0 & 0 \\ 0 & 0 \\ 1 & 0 \\ 0 & 0 \\ 0 & 0 \\ 0 & 1 \end{bmatrix}$						$B = \begin{bmatrix} 0 & 0 \\ 0 & 0 \\ 1 & 0 \\ 0 & 0 \\ 0 & 0 \\ 0 & 1 \end{bmatrix}$					
$C = \begin{bmatrix} 1 & 1 & 0 & 0 & 0 & 0 \end{bmatrix}$						$C = \begin{bmatrix} 1 & 1 & 0 & 0 & 0 & 0 \end{bmatrix}$					

$$\frac{dE_V}{dt} = \phi I - \delta_V E_V, \tag{17}$$

$$\frac{dE_T}{dt} = \frac{\beta_T(U + I)}{k + (U + I)} - \delta_T E_T, \tag{18}$$

$$\frac{dC}{dt} = u_2(t) - \psi C. \tag{19}$$

**3.1. Design of continuous controller**

In this section, a tracking continuous controller is designed based on the EESA method. This control method is suitable for linear, time-invariant, multi-inputs systems. In this approach, the control gain ( $k$ )

assigns both the spectrum of closed-loop eigenvalues and their associated set of eigenvectors, leading to the desired time response characteristics.

The relation between closed-loop eigenvalues ( $\lambda$ ) and eigenvectors ( $\nu$ ) is shown in the following equation, in which  $A$  and  $B$  represent the state-space matrices:

$$[A + Bk] \nu_i = \lambda_i \nu_i, \tag{20}$$

Eq. (20) can be re-written into the following equation, where  $q$  is the ratio of eigenvectors:

$$[A - \lambda_i I \quad B] \begin{bmatrix} \nu_i \\ q_i \end{bmatrix} = 0 \quad \text{for } i=0, 1, \dots, n. \tag{21}$$

**Table 6.** Eigenvalues of the equilibrium points shown in Table 5.

Equilibrium point	Eigen value	Eigen vector
First	$\begin{bmatrix} -4.17 & -1.2758 & -0.009 & 0.4959 \\ & & -0.0054 + 0.043i & -0.0054 - 0.043i \end{bmatrix}$	$\begin{bmatrix} 0 & 0.02 & 0.0055 & -1 & 0.5315 & 0.4628 \\ 0 & -0.0054 & 0.0021 & 0 & 0 & 0 \\ 0 & 1 & 1 & 0 & 0 & 0 \\ 1 & 0.031 & 0.0031 & 0 & 0 & 0 \\ 0 & 0 & 0 & 0 & -0.0001 & 0 \\ 0 & 0 & 0 & 0 & 0 & 0.8471 \end{bmatrix}$
Second	$\begin{bmatrix} -4.17 & -44.537 & -0.0097 + 0.0041i \\ & & -0.0097 - 0.0041i & -0.0049 + 0.043i & -0.0049 - 0.043i \end{bmatrix}$	$\begin{bmatrix} 0 & 0.0661 + 0.3173i & 0.0661 - 0.3173i \\ 0.1935 & 0.0002i & -0.0002i \\ -0.9811 & 0.9460 & 0.9460 \\ -0.003 & 0.0037 - 0.0002i & 0.0031 + 0.0002i \\ 0 & 0 & 0 \\ 0 & 0 & 0 \\ 0.0007 - 0.0057i & 0.0007 + 0.0057i & 0.4628 \\ 0 & 0 & 0.0003 \\ 1 & 1 & -0.0134 \\ 0.0028 - 0.0015i & 0.0028 + 0.0015i & -0.0001 \\ 0 & 0 & 0 \\ 0 & 0 & 0.8863 \end{bmatrix}$

To satisfy Eq. (21),  $[v_i^T \ q_i^T]^T$  must lie in the null space of matrix  $S$ , while:

$$S(\lambda_i) = [A - \lambda_i I \ B] \quad \text{for } i = 0, 1, \dots, n. \quad (22)$$

By deriving the null space of the matrix  $S$ , the value of  $q_i$  is determined. Thus, the control gain can be calculated via Eq. (23) as follows:

$$k = [q_1 \ q_2 \ \dots \ q_n] [v_1 \ v_2 \ \dots \ v_n]^{-1}. \quad (23)$$

The selected eigenvectors must be linearly independent; thus, the inverse matrix exists. In this method, the shape of a mode is determined by eigenvector and its time-domain characteristic is specified by eigenvalues.

Eqs. (20)–(23) show the regulator controller, which mainly stabilizes an unstable open-loop system. However, in this paper, a trajectory controller is desired

and it makes the output vector ( $w$ ) track the reference input vector ( $r$ ) as follows:

$$\lim_{t \rightarrow \infty} w(t) = r. \quad (24)$$

A new signal  $z$  is defined, which shows the difference between the output and the command desired input. The new composite system can be governed by Eq. (25), where  $A, B$ , and  $C$  are the matrices in the state space equation of the system as follows:

$$\begin{bmatrix} \dot{x} \\ \dot{z} \end{bmatrix} = \begin{bmatrix} A & 0 \\ -C & 0 \end{bmatrix} \begin{bmatrix} x \\ z \end{bmatrix} + \begin{bmatrix} B \\ 0 \end{bmatrix} u + \begin{bmatrix} 0 \\ I \end{bmatrix} r. \quad (25)$$

The first row in Eq. (25) is derived from the first equation of state space and the second one can be obtained by differentiating  $z$ . Therefore, the new state-space matrices are defined as follows:

$$A' = \begin{bmatrix} A & 0 \\ -C & 0 \end{bmatrix}, \quad B' = \begin{bmatrix} B \\ 0 \end{bmatrix}, \quad C' = [C \quad 0]. \quad (26)$$

By solving Eq. (26),  $x$  and  $z$  converge to zero. Thus, the output vector tracks the command input and Eq. (24) is satisfied [32].

### 3.2. Design of discrete control

In this section, a discrete tracking controller is designed, which is more feasible than the continuous one. Continuous state-space matrices are converted into the discrete ones. Then, the discrete EESA control method is designed and applied to the continuous system using Zero-Order Hold (ZOH) approach. ZOH assumes that the input vector ( $u(t)$ ) only changes at equally spaced sampling instants. The first discrete state-space equation is:

$$x((k + 1)T) = G(T)x(kT) + H(T)u(kT), \quad (27)$$

where the new state-space matrices  $G$  and  $H$  are dependent on sampling period  $T$  at time  $k$ . The input vector is assumed constant over the time interval between  $kT$  and  $(k + 1)T$ . Thus, the solution to the continuous system is:

$$x((k + 1)T) = e^{AT}x(kT) + \int_0^T e^{A(T-\lambda)}Bu(kT)d\lambda. \quad (28)$$

By comparing Eq. (28) with the continuous time response,  $G$  and  $H$  are:

$$G(T) = e^{AT}, \quad H(T) = \left( \int_0^T e^{A(T-\lambda)}d\lambda \right) B. \quad (29)$$

Under the condition where  $A$  is not singular,  $H$  can be simplified to:

$$H = A^{-1}(e^{AT} - 1)B. \quad (30)$$

Therefore, the EESA method is employed using the discrete state-space matrices  $G$  and  $H$  to design a discrete controller. Ogata [33] elaborated on more details of Eqs. (27) to (30). It is also desired to apply the controller to the continuous system using ZOH approach.

The numerical results are shown in Table 7. There are some optimization approaches to finding the desired closed-loop poles such as [34] in which the cost function maximizes the H-infinity norm of the unstructured stability and the robustness norm of the closed-loop model. However, this study finds the desired poles based on experience, as suggested in [33]. We use the command “place” in MATLAB to find the control

gain based on the EESA method. The optimization algorithm in [34] was employed to create a suitable eign structure of the model and choose the optimal eign vector. It minimizes the sensitivity of the assigned poles to perturbations in the system and gain matrices as well as the upper bounds on the norm of the feedback matrix and on the transient response and maximizes a lower bound on the stability margin.

### 4. Tracking control simulations and results

In this section, a 6-state chemovirotherapy model is used. The equations are linearized around the second equilibrium point, as given in Table 5. Continuous and discrete controllers were designed and applied to the nonlinear model using EESA method. In experimental studies, virotherapy is a successful treatment, provided that the overall tumor masses are low and stabilized [7]. This condition is met when the initial condition is close to the stabilized equilibrium point.

The average value of parameters in equations is selected so that the parametric uncertainties can be disregarded. The 4th-order Runge-Kutta uses an iterative method in MATLAB for simulating the closed-loop system.

#### 4.1. Simulations of the continuous controller and results

It is desired to reduce the tumor densities as soon as possible with limited control inputs. As in tracking problems, the system output is desired to track the command input. Therefore, selecting an appropriate command input can satisfy the demands. Figure 1 shows the block diagram.

In order to determine an appropriate command input, it was assumed that the command input would have three main attributes: the slope, Sampling Step Interval (SSI), and the shape of the command input. Achieving optimal values for the attributes results in an optimal command input. First, different command inputs with different slopes were compared. The proper slope for the command input was selected to produce less fluctuations in the trajectories. In other words, the cost function is the error between a trajectory and the command input and the best value of the slope is defined to minimize the cost function.

The optimal SSI and optimal shape were determined using the same method. In this paper, the command input is a stair function with a negative slope. Results are compared with the exponential command

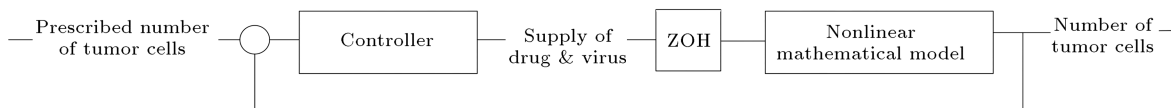
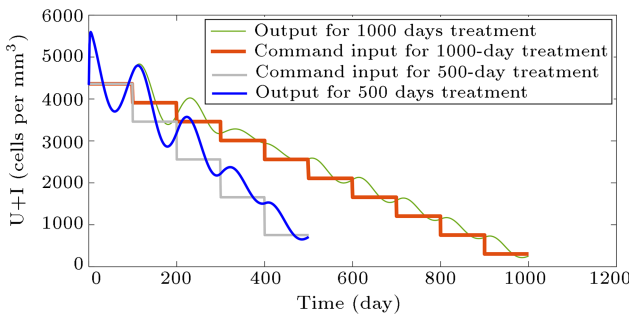


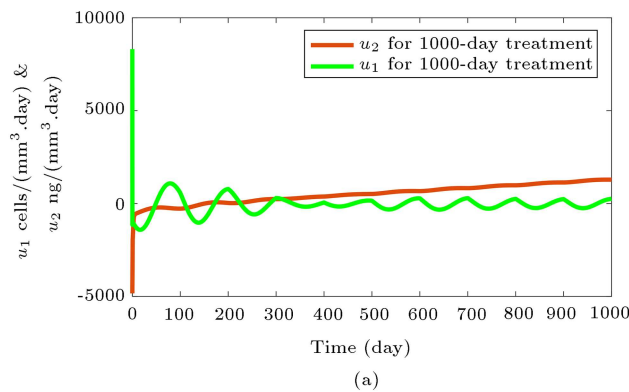
Figure 1. The block diagram of the closed-loop control system.

**Table 7.** Numerical values of the state metrics, their desired poles, kernel metrics, and gain vectors.

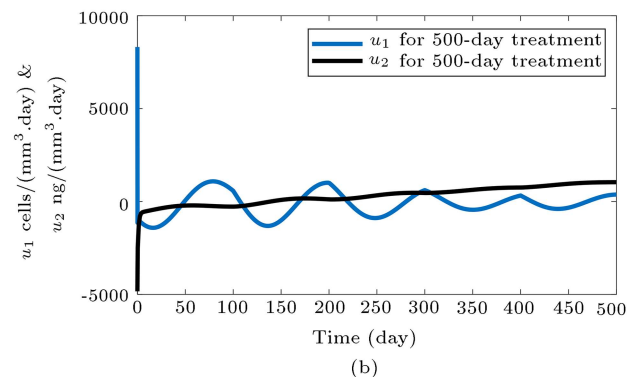
State-space matrices	$A' =$	$\begin{bmatrix} 0.00043 & -0.0008975 & -0.00021 & - & -348.57 & -2.178 & 0 \\ 0.0306 & -44.53 & 0.0021 & -0.626 & -0.3129 & -0.00187 & 0 \\ -0.0306 & 225.75 & -0.0121 & 0 & 0 & 0 & 0 \\ 0 & 0.7 & 0 & -0.01 & 0 & 0 & 0 \\ 0.0000045 & 0.0000045 & 0 & 0 & -0.01 & 0 & 0 \\ 0 & 0 & 0 & 0 & 0 & -4.17 & 0 \\ -1 & -1 & 0 & 0 & 0 & 0 & 0 \end{bmatrix}$
	$B' =$	$\begin{bmatrix} 0 & 0 \\ 0 & 0 \\ 1 & 0 \\ 0 & 0 \\ 0 & 0 \\ 0 & 1 \\ 0 & 0 \end{bmatrix}$
	$C' =$	$\begin{bmatrix} 1 & 1 & 0 & 0 & 0 & 0 & 0 \end{bmatrix}$
	$G =$	$\begin{bmatrix} 0.9995 & -0.0104 & -0.0021 & 0.0032 & -346.8013 & -0.5141 \\ 6.8596e-4 & 1.0477e-5 & 4.5232e-5 & -0.0139 & -0.2398 & -35307e-4 \\ 0.1202 & 5.0132 & 0.9981 & -3.07 & -21.893 & -0.0498 \\ 4.6758e-4 & 0.0156 & 3.1454e-5 & 0.9805 & -0.0844 & 1.9239e-4 \\ 4.4802e-6 & 7.7227e-8 & -4.5038e-9 & -5.6575e-8 & 0.9893 & -1.7892e-6 \\ 0 & 0 & 0 & 0 & 0 & 0.0155 \end{bmatrix}$
	$H =$	$\begin{bmatrix} -0.001 & -0.399 \\ 4.5156e-5 & -2.76e-4 \\ 0.999 & -0.0209 \\ 1.5515e-5 & -8.0381e-5 \\ -1.4705e-9 & -7.4302e-7 \\ 0 & 0.2361 \end{bmatrix}$
Assigned poles		$\begin{bmatrix} -4 & -45 & -0.01 + 0.004i & -0.01 - 0.004i & -0.005 + 0.05i & -0.005 - 0.05i & -1 \end{bmatrix}$
Kernel matrix for Ah		$\begin{bmatrix} 0 \\ 0 \\ 0 \\ 0 \\ 0 \\ 0 \\ 1 \end{bmatrix}$
Kernel matrix for Gh		$\begin{bmatrix} 0 \\ -0.19 \\ 0.9632 \\ 0.03 \\ 0 \\ 0 \\ -0.1899 \end{bmatrix}$
Discrete controller gain vector	$K =$	$\begin{bmatrix} -0.1534 & 0.5485 & 0.0206 & 23.9343 & 1.442e3 & 0.193 & -0.0401 \\ -1.173 & 0.2584 & 0.0418 & 3.6814 & 2.4858e3 & 0.6062 & 6.2802e-4 \end{bmatrix}$
Continuous controller gain vector	$K =$	$\begin{bmatrix} -678.0243 & 9.8645e5 & -46.5407 & 1.385e4 & 1.0034e4 & 7.8408 & -0.0017 \\ -0.1654 & -926.4937 & 0.0408 & 16.7156 & 3.7451e4 & -6.5447 & 0.0082 \end{bmatrix}$



**Figure 2.** The effect of command input slope on tumor density reduction in the continuous model.



(a)



(b)

**Figure 3.** The effect of command input slope on drug and virus usage in the continuous model: (a) 1000 days and (b) 500 days.

input and it is demonstrated that the stair function is of better selection. The steeper slope the command input, the shorter the treatment duration and the lower the drug dosage, but the higher the virus dosage. An optimal command input slope is determined that compromises the demands. In Figures 2 and 3, two command input slopes are compared.

The patient’s age contributes to the treatment duration [35,36]. Elderly’s immune system is not as strong as the young’s; therefore, preserving the number of healthy cells is more important than reducing the tumor densities. Hence, the steeper slope is devoted to the young.

These treatment durations are within the allowable interval [37]. This may take longer than

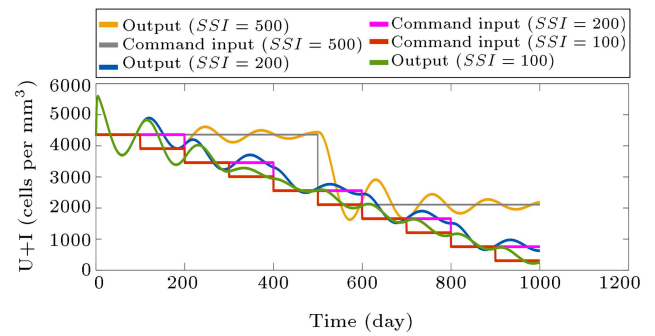


**Figure 4.** The effect of sampling step interval on tumor density reduction in the continuous model.

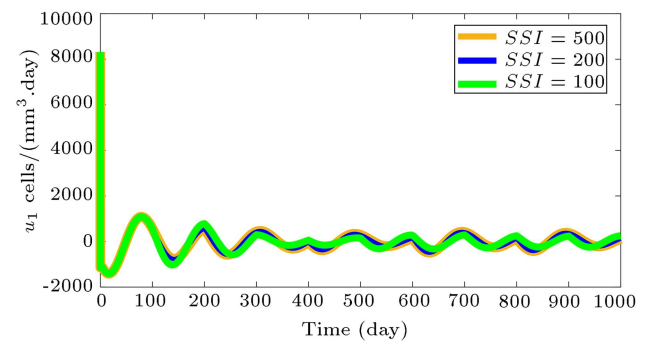


**Figure 5.** The effect of sampling step interval on virus dosage ( $u_1$ ) in the continuous control system.

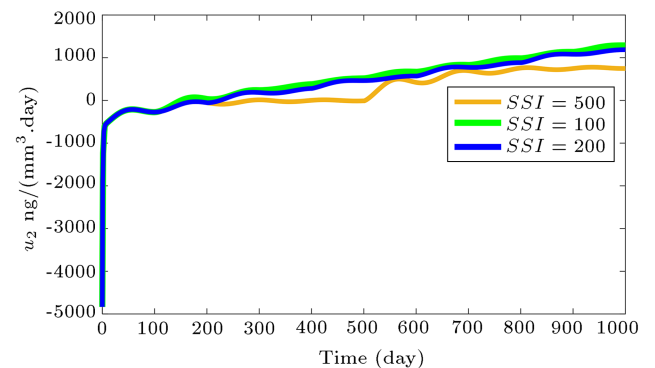


**Figure 6.** The effect of sampling step interval on drug dosage ( $u_2$ ) in the continuous control system.

other cancer treatments since the immune cells in the virotherapy need a longer time to reduce the tumor density [38,39]. Treatment taking more than 1000 days makes the drug dosage out of range. Thus, 1000 days is the optimal treatment duration for the elderly with the maximum drug dosage of approximately 1200 Nanograms per  $\text{mm}^3$  per day and virus dosage of 230 virions per  $\text{mm}^3$  per day.

The SSI plays an important role in the tracking efficiency. Figures 4, 5, and 6 show constant treatment duration of 1000 days as well as the effect of SSI on output and inputs of the plant.

SSI does not affect the maximum virus dosage, but can reduce maximum drug dosage by 540

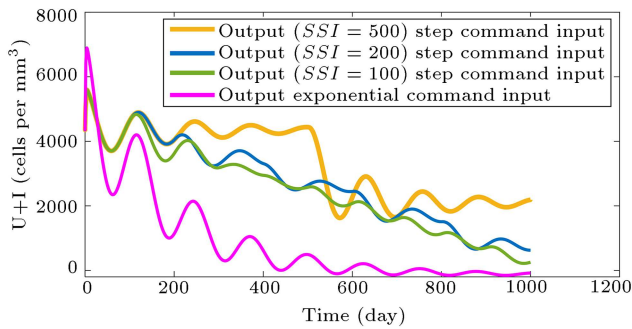


**Figure 7.** The effect of command input slope on tumor density reduction in the continuous model.

Nanograms per  $\text{mm}^3$  per day, as it increases from 100 to 500. Figure 4 shows that  $SSI = 500$  gives the output a greater chance to follow the command input. However, it experiences more fluctuations than other SSIs. As a result,  $SSI = 200$  would be the best choice as it causes the number of tumors declines more smoothly. The smoother trajectory refers to the one that has less error than the desired command input.

Figures 7 and 8 evaluate the effect of command input. The stair function as the desired command input leads to less fluctuation in the output of the closed-loop system with less control inputs of the plant.

**4.2. Simulations of the discrete controller and results**

Eq. (29) shows that  $G$  and  $H$  are dependent on not only the continuous state space matrices but also  $T$ .

Patients may undergo chemotherapy in cycles, which is a periodic treatment schedule followed by a resting period. One of the common schedules utilized is to give chemotherapy with a constant dosage every day during a week and to stop the treatment for 3 weeks

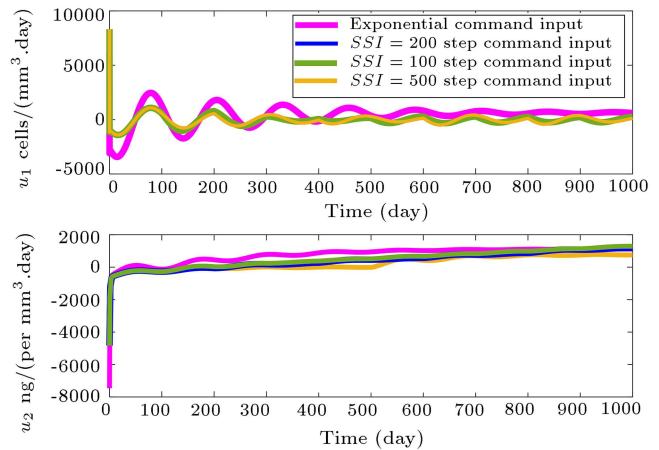


**Figure 8.** The effect of command input slope on drug and virus usage in the continuous model.

to allow the patient’s body to be recovered. This one-month treatment is considered a cycle.

The referenced study [5] found that adenovirus and measles viruses were used in the combination of chemotherapy and virotherapy. Table 8 represents a summary of these 2 types of viruses and suitable  $T$  for them.

The effect of  $T$  on output and inputs of the plant is evaluated in Figures 9 and 10.  $T$  less than 1 does not have an experimental meaning, owing to the level of tolerance in the human body. The negative values for the virus in Figure 10 confirm the impossibility of injecting the drug and virus every day. In Figure 9, as  $T$  increases from 1 up to 20, the tracking behavior becomes more smooth with fewer fluctuations. However, at  $T = 25$ , fluctuations begin to increase insofar as  $T = 44$  at which the dynamic system becomes unstable. As a theoretical clarification of the unstable system, the

**Table 8.** Chemovirotherapy description with two different types of viruses.

Type of virus	Combination [47]	Drug dosage [47]	Treatment duration [47]	$T$ [39]
Adenovirus	Ad5/3MDR1E1	Doxorubicin:	After 96 h, 10% fixed	*Single shot *Triple-hit course *Every 4 weeks (up to 6 courses)
		initially: 10 ng/ml		
		weekly increase: 10 ng/ml		
		Max dose: 150 ng/ml		
Measles	MeV(CD46)	cisplatin:	After 72 h, 40% fixed	*Single shot *Two-hit course *Every 4 weeks (up to 6 courses)
		initially: 10 ng/ml		
		weekly increase: 5 ng/ml		
		Max dose: 40 ng/ml		

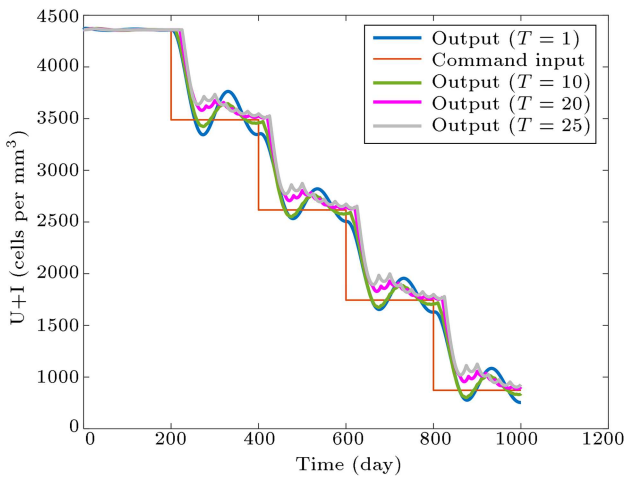


**Figure 9.** The effect of sampling instant on tumor density reduction in the discrete model.

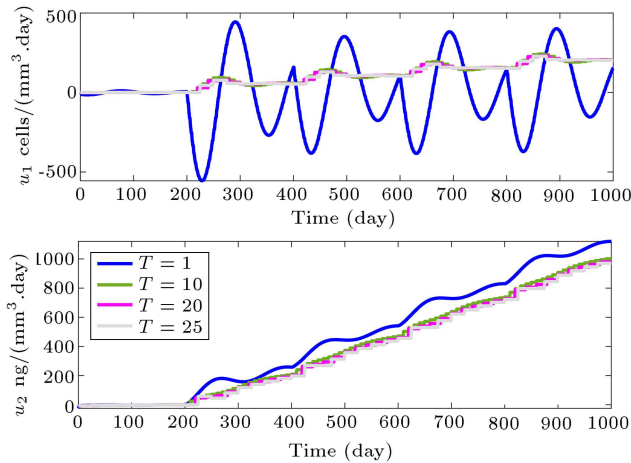


**Figure 10.** The effect of sampling instant on drug and virus usage in the discrete model.

output of the unstable system does not converge to the desired command input. For clarification, the number of cancer cells in the patient body will rise dramatically.

On the other hand, as shown in Figure 10, as  $T$  increases from 1 to 10, fluctuations in  $u_1$  and the amount of  $u_2$  are reduced. However, a rise in the value of  $T$  from 10 to 25 does not have much effect on the plant inputs. Consequently, the best sampling instant is 20 days, which means that patients should receive drugs and viruses every 20 days.

#### 4.3. Comparison between the continuous and discrete controllers in simulations

Both of the controlled systems have been simulated in a digital computer and have not been applied to an analog system with nonlinear behavior. In the discrete controller, the inputs of the plant are applied discretely, which make the simulation more realistic.

Based on the results in Figures 11 and 12 and their comparison in Table 9, the system behaves more smoothly in the presence of a discrete controller.

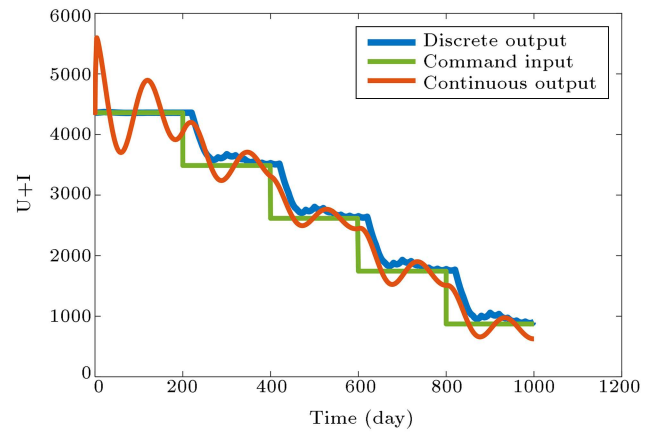


**Figure 11.** Comparison of the trajectory of tumor density in the continuous and discrete models.

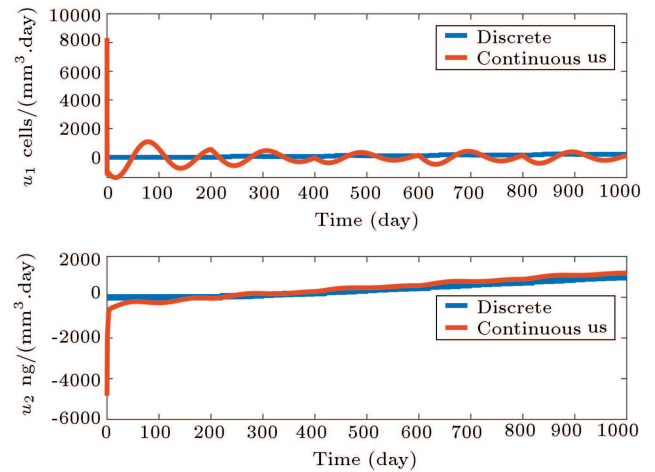


**Figure 12.** Comparison of the amount of drug and virus usage in the continuous and discrete models.

## 5. Conclusions

In this paper, a nonlinear mathematical model of the human body under chemovirotherapy was considered. This model simulates the infected and uninfected tumor cells, free viruses, chemotherapeutic drugs, and immune cells. Thus, in our simulations, the impact of immune cells on cancer treatment is examined. This model is linearized around a reasonable realistic equilibrium point.

A linear tracking controller based on EESA method was designed continuously and discretely. The controller was applied to the nonlinear model based on ZOH approach, showing the robustness of the controller against the nonlinearities of the model. The objective is to find a minimum treatment duration with a limited number of control inputs. Regulation of the command input characteristics provided us with the opportunity to form agreement between the former and the desired demands. The following results can be extracted:

- ✓ The steeper the command input, the shorter the

**Table 9.** Comparison of the performance of the continuous and discrete systems.

	Trajectory of tumor's density	Drug usage	Virus usage
Continuous	Fluctuations in the beginning Noticeable steady state error	Increase with steeper slope	Fluctuating value
Discrete	No fluctuations in the beginning Small steady state error	Increase with more gradual slope	Almost a constant value

treatment duration, but the higher the drug dosage. Therefore, by regulating these factors, the optimal treatment can be investigated;

- ✓ The SSI of the command input would affect the behavior of the plant inputs. Larger SSI provided the chance to the output to track the command input more smoothly. However, in this case, the tumor density was reduced. The optimal SSI proposed in this paper was 200;
- ✓ As drug and virus are injected into the body from time to time, the results of the discrete controller are more reasonable and realistic. The discrete controller behaves more smoothly and control inputs of the plant experience less fluctuation than the continuous one. Within 1000 days, with the limited drug and virus dosage, the discrete controller can reduce the tumor densities by 3500 cells per  $\text{mm}^3$ ;
- ✓ The important factor that contributes to the discretization is sampling instant ( $T$ ). The optimal sampling instant was suggested to be 20 days, since smaller sampling instants would result in more fluctuations in drug and virus consumption pattern and larger sampling instants bring about instability.

The initiation of this treatment was restricted to the vicinity of equilibrium points. The controllers also become unstable due to the cycles and schedulable  $T$  as well as parameter uncertainties. Based on the results, the linear controller cannot efficiently converge the steady state error to zero. To improve its efficiency, in the future work, robust nonlinear controllers [38,40] can be applied to the model to make the results more general. Moreover, some states cannot be measured in the model, experimentally. Therefore, in the future, designing appropriate observers can ensure more sensible results.

#### Acknowledgment

The authors acknowledge the “Research Office of Sharif University of Technology, Tehran, Iran” for supporting this research through the grant program # QB980923.

#### References

1. Cause, G.D. and Age, S., *By Country and by Region, 2000-2019*, World Health Organization (2020).
2. Head, B., Harris, L., Kayser, K., et al. “Coping with the financial consequences of cancer”, *Supportive Care in Cancer*, **26**(3), pp. 975–987 (2018).
3. Organization, W.H., *Global Tuberculosis Report 2013*, World Health Organization (2013).
4. André, T., Colin, P., Louvet, C., et al. “Semimonthly versus monthly regimen of fluorouracil and leucovorin administered for 24 or 36 weeks as adjuvant therapy in stage II and III colon cancer: results of a randomized trial”, *Journal of Clinical Oncology*, **21**(15), pp. 2896–2903 (2003).
5. Ungerechts, G., Engeland, C.E., Buchholz, C.J., et al. “Virotherapy research in Germany: from engineering to translation”, *Human Gene Therapy*, **28**(10), pp. 800–819 (2017).
6. Nguyen, A., Ho, L., and Wan, Y. “Chemotherapy and oncolytic virotherapy: advanced tactics in the war against cancer”, *Frontiers in Oncology*, **4**, p. 145 (2014).
7. Binz, E. and Lauer, U.M. “Chemovirotherapy: Combining chemotherapeutic treatment with oncolytic virotherapy”, *Oncolytic Virotherapy*, **4**, p. 39 (2015).
8. Bartee, E. “Potential of oncolytic viruses in the treatment of multiple myeloma”, *Oncolytic Virotherapy*, **7**, p. 1 (2017).
9. Biotech, O. “Inc. announces additional data from REO 018 randomized study of REOLYSIN<sup>®</sup> in head and neck cancers 2014” (2019).
10. Biotech, O. “Oncolytics Biotech Inc. announces additional data from REO 018 randomized study of REOLYSIN in head and neck cancers [press release]”, Oncolytics Biotech (2014).
11. Malinzi, J. “Mathematical analysis of a mathematical model of chemovirotherapy: effect of drug infusion method”, *Computational and Mathematical Methods in Medicine*, **86**, pp. 97–100 (2019).
12. Magi, S., Iwamoto, K., and Okada-Hatakeyama, M. “Current status of mathematical modeling of cancer - from the viewpoint of cancer hallmarks”, *Current Opinion in Systems Biology*, **2**, pp. 39–48 (2017).

13. Eftimie, R., Bramson, J.L., and Earn, D.J.D. “Interactions between the immune system and cancer: A brief review of non-spatial mathematical models”, *Bulletin of Mathematical Biology*, **73**(1), pp. 2–32 (2011).
14. Martin, R.B., Fisher, M.E., Minchin, R.F., et al. “A mathematical model of cancer chemotherapy with an optimal selection of parameters”, *Mathematical Biosciences*, **99**(2), pp. 205–230 (1990).
15. Panetta, J.C. and Adam, J. “A mathematical model of cycle-specific chemotherapy”, *Mathematical and Computer Modelling*, **22**(2), pp. 67–82 (1995).
16. Pontryagin, L.S., *Mathematical Theory of Optimal Processes*, Routledge (2018).
17. Zietz, S. and Nicolini, C. “Mathematical approaches to optimization of cancer chemotherapy”, *Bulletin of Mathematical Biology*, **41**(3), pp. 305–324 (1979).
18. Wang, P., Liu, R., Jiang, Z., et al. “The optimization of combination chemotherapy schedules in the presence of drug resistance”, *IEEE Transactions on Automation Science and Engineering*, **16**(1), pp. 165–179 (2018).
19. de Pillis, L., Renee Fister, K., Gu, W., et al. “Mathematical model creation for cancer chemimmunotherapy”, *Computational and Mathematical Methods in Medicine*, **10**(3), pp. 165–184 (2009).
20. Liu, W. and Freedman, H. “A mathematical model of vascular tumor treatment by chemotherapy”, *Mathematical and Computer Modelling*, **42**(9–10), pp. 1089–1112 (2005).
21. Pinho, S.T.R.d., Freedman, H., and Nani, F. “A chemotherapy model for the treatment of cancer with metastasis”, *Mathematical and Computer Modelling*, **36**(7–8), pp. 773–803 (2002).
22. Dehingia, K., Sarmah, H.K., and Jeelani, M.B. “A brief review on cancer research and its treatment through mathematical modelling”, *Ann Cancer Res Ther*, **29**, pp. 34–40 (2021).
23. Malinzi, J., Eladdadi, A., and Sibanda, P. “Modelling the spatiotemporal dynamics of chemovirotherapy cancer treatment”, *Journal of Biological Dynamics*, **11**(1), pp. 244–274 (2017).
24. Swan, G.W. and Vincent, T.L. “Optimal control analysis in the chemotherapy of IgG multiple myeloma”, *Bulletin of Mathematical Biology*, **39**(3), pp. 317–337 (1977).
25. Shi, J., Alagoz, O., Erenay, F.S. et al. “A survey of optimization models on cancer chemotherapy treatment planning”, *Annals of Operations Research*, **221**(1), pp. 331–356 (2014).
26. Coldman, A.J. and Murray, J. “Optimal control for a stochastic model of cancer chemotherapy”, *Mathematical Biosciences*, **168**(2), pp. 187–200 (2000).
27. Malinzi, J., Ouifki, R., Eladdadi, A., et al. “Enhancement of chemotherapy using oncolytic virotherapy: mathematical and optimal control analysis”, arXiv preprint arXiv:1807.04329 (2018).
28. Wodarz, D. and Komarova, N. “Towards predictive computational models of oncolytic virus therapy: basis for experimental validation and model selection”, *PLoS One*, **4**(1), p. e4271 (2009).
29. Tian, J.P. “The replicability of oncolytic virus: defining conditions in tumor virotherapy”, *Mathematical Biosciences and Engineering*, **8**(3), pp. 841–860 (2011).
30. Kuznetsov, V.A., Makalkin, I.A., Taylor, M.A., et al. “Nonlinear dynamics of immunogenic tumors: parameter estimation and global bifurcation analysis”, *Bulletin of Mathematical Biology*, **56**(2), pp. 295–321 (1994).
31. Pinho, S.T.R., Rodrigues, D.S., and Mancera, P.F.D.A. “A mathematical model of chemotherapy response to tumour growth”, *Canadian Applied Mathematics Quarterly*, **19**(4), pp. 369–828 (2011).
32. d’Azzo, J.J. and Houpis, C.D., *Linear Control System Analysis and Design: Conventional and Modern*, McGraw-Hill Higher Education (1995).
33. Ogata, K., *Discrete-Time Control Systems*, Prentice Hall Englewood Cliffs, 2nd Edn. (1995).
34. Kautsky, J., Nichols, N.K., and Van Dooren, P. “Robust pole assignment in linear state feedback”, *International Journal of Control*, **41**(5), pp. 1129–1155 (1985).
35. Kourelis, K., Tsue, T., Girod, D., et al. “Negative prognostic factors for head and neck cancer in the young”, **21**, pp. 459–464 (2013).
36. Li, Y., Chu, Y., Song, R., et al. “Thalidomide combined with chemotherapy in treating elderly patients with advanced gastric cancer”, *Ageing Clinical and Experimental Research*, **30**(5), pp. 499–505 (2018).
37. Guntinas-Lichius, O., Wendt, T., Buentzel, J., et al. “Head and neck cancer in Germany: a site-specific analysis of survival of the Thuringian cancer registration database”, *Journal of Cancer Research and Clinical Oncology*, **136**(1), pp. 55–63 (2010).
38. Lauer, U. and Binz, E. “Chemovirotherapy: combining chemotherapeutic treatment with oncolytic virotherapy”, *Oncolytic Virotherapy*, **4**(1), pp. 39–48 (2015).
39. Ruf, B. and Lauer, U.M. “Assessment of current virotherapeutic application schemes: “hit hard and early” versus “killing softly”?”, *Molecular Therapy-Oncolytics*, **2**, p. 15018 (2015).
40. Mobaraki, M. and Moradi, H. “Design of robust control strategy in drug and virus scheduling in nonlinear process of chemovirotherapy”, *Computers & Chemical Engineering*, **150**, 107318 (2021).
41. Bajzer, Ž., Carr, T., Josić, K., et al. “Modeling of cancer virotherapy with recombinant measles viruses”, *Journal of Theoretical Biology*, **252**(1), pp. 109–122 (2008).

42. Kirschner, D. and Panetta, J.C. “Modeling immunotherapy of the tumor-immune interaction”, *Journal of Mathematical Biology*, **37**(3), pp. 235–252 (1998).
43. Brock, T.D. “The emergence of bacterial genetics”, *Cold Spring Harbor Laboratory Press Cold Spring Harbor, NY* (1990).
44. Bollard, C.M. and Heslop, H.E. “T cells for viral infections after allogeneic hematopoietic stem cell transplant”, *Blood*, **127**(26), pp. 3331–3340 (2016).
45. Gajewski, T.F., Schreiber, H., and Fu, Y.-X. “Innate and adaptive immune cells in the tumor microenvironment”, *Nature Immunology*, **14**(10), p. 1014 (2013).
46. Le, D., Miller, J.D., and Ganusov, V.V. “Mathematical modeling provides kinetic details of the human immune response to vaccination”, *Frontiers in Cellular and Infection Microbiology*, **4**, p. 177 (2015).
47. Rein, D.T., Volkmer, A., Bauerschmitz, G., et al. “Combination of a MDR1-targeted replicative adenovirus and chemotherapy for the therapy of pretreated ovarian cancer”, *Journal of Cancer Research and Clinical Oncology*, **138**(4), pp. 603–610 (2012).
48. Weiland, T., Lampe, J., Essmann, F., et al. “Enhanced killing of therapy-induced senescent tumor cells by oncolytic measles vaccine viruses”, *International Journal of Cancer*, **134**(1), pp. 235–243 (2014).

## Biographies

**Mobina Mobaraki** received BSc in Mechanical Engineering from Shahid Beheshti University (SBU) in 2018 and MSc in Applied Mechanics from Sharif University of Technology (SUT), Tehran, Iran in 2020. Currently, she is doing her PhD in Electrical and Computer Engineering, the University of British Columbia (UBC), Vancouver, British Columbia, Canada. Her current research interests include artificial intelligence, machine learning, and computer vision. Her research interests include robotics and control engineering.

**Hamed Moradi** received BSc in Mechanical Engineering degree specializing in Solid Mechanics from Amirkabir University of Technology in 2005; MSc and PhD in Applied Mechanics from Sharif University of Technology (SUT), Tehran, Iran in 2008 and 2012. Currently, he is an Associate Professor at the Department of Mechanical Engineering, Sharif University of Technology. His current research interests include the modeling of dynamic systems, application of robust, nonlinear, and optimal control methods in various dynamics systems such as manufacturing, bio-engineering, thermo-fluid industrial processes, and power plant engineering. Also, he investigates the analysis of nonlinear dynamics and chaos in various oscillatory phenomena, especially in two areas of thermo-fluid systems and machining chatter vibrations.